Nano Energy 103 (2022) 107813

Contents lists available at ScienceDirect

Nano Energy

journal homepage: www.elsevier.com/locate/nanoen

Correlation between frictional heat and triboelectric charge: *In operando* temperature measurement during metal-polymer physical contact

Dong Woo Lee [a,1], Dae Sol Kong [a,1], Jong Hun Kim [b,*], Sang Hyeok Park [a], Ying Chieh Hu [a], Young Joon Ko [a], Chan Bae Jeong [c], Seoku Lee [d], Joong Il Jake Choi [e], Gwan-Hyoung Lee [b,f,g,h], Minbaek Lee [a], Jeong Jae Wie [i,j], Ki Soo Chang [c], Jeong Young Park [e,k], Jong Hoon Jung [a,*]

[a] Department of Physics, Inha University, Incheon 22212, South Korea
[b] Department of Materials Science and Engineering, Seoul National University, Seoul 08826, South Korea
[c] Division of Scientific Instrumentation and Management, Korea Basic Science Institute, Daejeon 34133, South Korea
[d] Program in Environmental and Polymer Engineering, Inha University, Incheon 22212, South Korea
[e] Center for Nanomaterials and Chemical Reactions, Institute for Basic Science (IBS), Daejeon 34141, South Korea
[f] Research Institute of Advanced Materials (RIAM), Seoul National University, Seoul 08826, South Korea
[g] Institute of Engineering Research, Seoul National University, Seoul 08826, South Korea
[h] Institute of Applied Physics, Seoul National University, Seoul 08826, South Korea
[i] Department of Organic and Nano Engineering, Hanyang University, Seoul 04763, South Korea
[j] Human-Tech Convergence Program, Hanyang University, Seoul 04763, South Korea
[k] Department of Chemistry, Korea Advanced Institute of Science and Technology (KAIST), Daejeon 34141, South Korea

ARTICLE INFO

Keywords:
In operando measurement
Frictional heat
Triboelectric charge
Temperature variation
Activation energy
Young's modulus

ABSTRACT

In operando techniques have emerged to elucidate the fundamental mechanism of triboelectrification via relevant physical quantity measurement during the physical contact of two materials. Here, a correlation between frictional heat and triboelectric charge is reported in a metal-polymer triboelectric nanogenerator through the *in operando* temperature measurement. Fluorine-doped tin oxide (FTO) metal is slid back-and-forth under different contact pressures across polydimethylsiloxane (PDMS) polymers having different degrees of crosslinking, i.e., mixing ratio. Both the triboelectric charge and temperature variation increase and become saturated with different time-constants. Notably, the saturated triboelectric charge increases, while the saturated temperature decreases, with increasing mixing ratio. In contrast, both saturated triboelectric charge and temperature increase with increasing contact pressure. X-ray photoemission spectroscopy reveals that chemical bonds are modified inhomogeneously at the surface, and that charged materials are transferred from PDMS to FTO in accordance with the mixing ratio- and sliding time-dependent triboelectric charges. Frictional heat plays a distributive role in bond rupture and temperature variation, depending on the activation energy and frictional coefficient of PDMS. *In operando* temperature variation measurement provides important information on the specific bonds for triboelectrification and detailed charge-transfer process during physical contact.

1. Introduction

The rapid depletion of fossil fuels and climate change have prompted great interest in energy harvesting from the environment [1,2]. Among various renewable energy sources, in particular, wasted mechanical vibrations with low frequency have been effectively converted into electricity via recently developed triboelectric nanogenerators (TENGs) [3,4]. TENGs are flexible, light-weight, and cost-effective devices and are one of the most promising power sources for portable and wearable devices in the Internet of Things (IoT) era [5–12]. The performance of TENGs strongly depends on the triboelectric charges generated during the physical contact between two materials. However, the identity and transfer mechanism of triboelectric charge is still unclear and varies depending on the contacting materials [13–22].

In operando measurement can provide critical hints for triboelectrification via real-time and simultaneous investigation of

* Corresponding authors.
E-mail addresses: crony96@snu.ac.kr (J.H. Kim), jhjung@inha.ac.kr (J.H. Jung).
[1] These authors contributed equally to this work.

https://doi.org/10.1016/j.nanoen.2022.107813
Received 15 July 2022; Received in revised form 1 September 2022; Accepted 14 September 2022
Available online 15 September 2022

triboelectric charge and relevant physical quantities. There have been several important reports on such measurements. Li et al. reported the atomic featured photon emission spectra acquired during contact electrification [23]. They provided the evidence of electron transfer at the interface of two materials via careful analysis of the atomic spectrum at low pressure. Lin et al. reported the triboelectric charge decay behavior under ultraviolet illumination [24]. They demonstrated the release of electrostatic charges on a dielectric surface via detailed analysis of the wavelength and intensity-dependent decay. Bayketin et al. reported the evolution of surface charge and surface roughness during contact electrification [25]. They concluded the material-transfer dominated triboelectrification in a soft contacting material via X-ray photoelectron spectroscopy for the various polymers. However, there have been few reports on *in operando* measurement of frictional heat induced temperature variation during contact electrification. Frictional heat has been considered one of the most important parameters for the bond breaking/creation model of material-transfer [26] and the thermionic emission model of electron-transfer [27].

In this paper, triboelectric charge and temperature variation are simultaneously investigated during the sliding of FTO metal on PDMS polymers. Crosslink density and contact pressure are systematically varied for triboelectric charge, and a synchronized infrared (IR) camera and thermocouple are adopted for temperature variation. Sliding time-dependent triboelectric charge and temperature variation as well as surface-sensitive X-ray photoemission results reveal that frictional heat inhomogeneously modifies and breaks the chemical bonds of PDMS, depending on activation energy and contact pressure. The remaining frictional heat changes the temperature of FTO and PDMS. Such a distributive role of frictional heat results in increased triboelectric charge and decreased temperature variation, and vice versa. The temperature variation precedes triboelectric charge during sliding. The broken bonds and/or charged materials in PDMS are transferred to FTO for triboelectrification due to their large modulus difference.

2. Experimental section

2.1. Fabrication and characterization of PDMS

PDMS films were fabricated using a conventional hot-press method. The PDMS precursor and crosslinker (Merck KGaA, Korea) were mixed at various weight ratios and then degassed under vacuum for 30 min. A small amount of mixture was poured onto a glass substrate and thermal curing was performed at 75 °C for 6 h with an applied pressure of 30 MPa. The same processes were applied to all PDMS films to minimize the sensitive physical properties on growth conditions [28].

Crystallinity, surface morphology, and Young's modulus of PDMS films were characterized by X-ray diffraction (XRD, X′PERT-PRO, PANalytical), an atomic force microscopy (AFM, XE-7, PSIA) and scanning electron microscopy (SEM, SU 8010, Hitachi), and a nanoindenter (G200, KLA instrument), respectively [29]. The frictional coefficient and adhesion force were measured by atomic force microscopy (SPM100, RHK Tech.) in an ultra-high vacuum environment (1×10^{-9} Torr) [30,31]. The friction coefficient and adhesion force were obtained from the frictional force-load force spectrum, as shown in Fig. S1, Supporting Information, and by utilizing the value for a thermally grown SiO_2 wafer [32]. The adhesion force corresponded to the minimum force for the pull-off of tip from the surface. Frequency-dependent dielectric constant and temperature-dependent weight loss were measured by an LCR meter (4284 A, HP) and thermogravimetric analyzer (TGA, TG 209 F3, Netzsch), respectively. For the TGA measurement, the heating rate was fixed at 10 °C/min. Specific heat and thermal diffusivity of PDMS films were obtained using a differential scanning calorimeter (DSC 204 F1, Netzsch) and a laser flash analysis system (LFA 447, Netzsch), respectively. Thermal conductivity was obtained by multiplying the specific heat, density, and thermal diffusivity [33]. A K-type thermocouple and commercial IR camera (A35, FLIT) were used to estimate the temperature of FTO and PDMS, respectively. Before the temperature measurement using the IR camera, the emissivity of PDMS (~0.9) was obtained using an emissometer (TSS-5X, Japan Sensor Corp.). The chemical bonds of PDMS films were examined using an X-ray photoemission spectroscopy system with the option of a micrometer-sized X-ray beam (XPS, PHI 5000, Ulvac-Phi).

2.2. Triboelectric output measurement of FTO-PDMS TENGs

The triboelectric output performance was characterized using a custom sliding system, in which a linear motor was used to move an FTO metal (Sigma Aldrich) back-and-forth on PDMS polymers. The metallic conduction and mechanical stability of FTO were confirmed by the temperature-dependent sheet resistance and current-voltage curve, and the absence of scratches after sliding, respectively (Fig. S2, Supporting Information). The FTO and PDMS were attached to the top and bottom plates of a sliding machine and then slid at a frequency of 1.5 Hz with the variation of contact pressure. The electrical outputs of the FTO-PDMS TENGs were measured using a digital phosphor oscilloscope (DSOX2002A, KEYSIGHT), a programmable electrometer (6517, Keithley), and a low-noise current preamplifier (SR570, Stanford Research Systems).

2.3. Finite-element computer simulations

COMSOL Multiphysics 5.6 software was used to simulate the temperature variation of PDMS during sliding. A three-dimensional model was developed for precise simulation. The same geometry of FTO-PDMS TENG was used, i.e., PDMS with a dimension of 0.5 cm × 1 cm × 1 mm and FTO/glass with a dimension of 5 cm × 4 cm × 2 mm. A box of air (10 cm × 10 cm × 10 cm) was used to model the atmospheric conditions. Pulse-type frictional heat (~1.5 mW with 1.5 Hz) was applied to the PDMS having specific heat of 1.586 J/gK and thermal conductivity of 0.175 W/mK. A Heat Transfer in Solids and Fluids were used to compute the temperature distribution for a fine mesh number of 611,755.

3. Results and discussion

3.1. In operando measurement system for triboelectric charge and temperature variation

Fig. 1a shows a schematic illustration and an optical image of the *in operando* triboelectric charge and temperature measurement system. The operation of the system is shown in Movie S1, Supporting Information. The FTO metal and PDMS polymer were attached to the top and bottom plates, respectively, and the gap between the two plates was varied by a micrometer. A single-electrode mode was adopted to obtain stable triboelectric outputs. The PDMS film deposited on an electrode for the two-electrode mode was found to be peeled off during the sliding of FTO. The real-time temperature variation is simultaneously monitored for FTO metal using a thermocouple and for PDMS polymer using an IR camera. In particular, the operation of the IR camera is synchronized with the back-and-forth motion of the sliding machine (Fig. 1b). Namely, the IR camera is turned on only when the PDMS surface is exposed to air, and the temperature distribution at the surface is averaged for precise estimation of temperature.

Supplementary material related to this article can be found online at doi:10.1016/j.nanoen.2022.107813.

Fig. 1c shows a schematic diagram of the power generation mechanism and temperature variation of an FTO-PDMS TENG. When the FTO and PDMS come into contact, the former and the latter are positively and negatively charged, respectively [34]. When the FTO moves backward, positive charges in the FTO move to the ground to effectively screen the reduced negative charges in the PDMS. Conversely, positive charges move from the ground to the FTO, when the FTO moves forward. On the other hand, frictional heat is generated only when the FTO moves on the

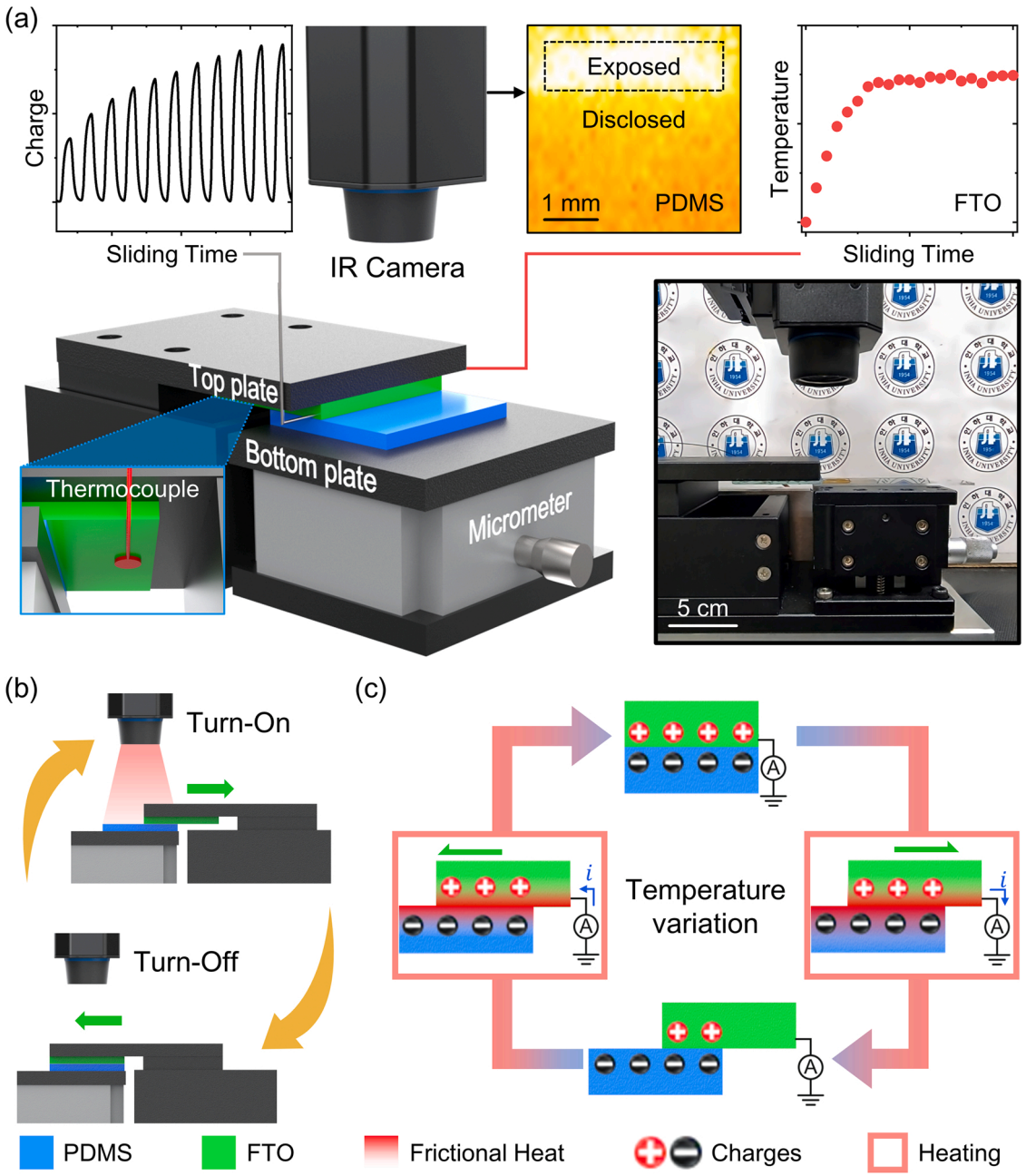

Fig. 1. *In operando* measurement system, and power- and frictional heat-generation mechanism. (a) Schematic illustration and optical image of an *in operando* measurement system for triboelectric charge and temperature during the sliding motion. Real-time temperatures are monitored using a thermocouple for the FTO metal and an infrared (IR) camera for the PDMS polymer. The contact pressure is varied by adjusting the gap between the top and bottom plates using a micrometer. (b) Synchronized operation of IR camera and sliding machine. The IR camera is operated only when the PDMS surface is exposed. (c) Schematic power generation mechanism and frictional heat generation process. Positive free charges (red circles) in the FTO flow back-and-forth to the ground and screen the negative bound charges (black circles) in the PDMS. Frictional heat is generated when the FTO slides on the PDMS polymer, as marked by red boxes, and temperature varies during a sliding cycle.

PDMS surface. Heating occurs twice in the FTO-PDMS TENG during one cycle of sliding, i.e., pulse-type heat. The frictional heat causes a continuous change of temperature, as confirmed by the computer simulation (Fig. S3 and Movie S2, Supporting Information).

Supplementary material related to this article can be found online at doi:10.1016/j.nanoen.2022.107813.

3.2. Mechanical, thermal, morphological, and dielectric properties of PDMS polymers

For the systematic understanding of the correlation between triboelectric charge and temperature variation, PDMS polymers were synthesized with various mixing ratios. Here, the mixing ratio represents the weight ratio of PDMS precursor to crosslinker [35]. Since the PDMS precursor has two vinyl end groups to react with a crosslinker, the mixing ratio could affect the mechanical, thermal, morphological, and dielectric properties of PDMS.

Fig. 2a shows the mixing ratio-dependent Young's modulus of the PDMS polymers. When the mixing ratio varies from 5:1–30:1, the modulus drastically decreases from 4.5 MPa for the former to 1.7 MPa for the latter. Such a large modification is attributed to the sharp increase of soft amorphous phase in the polymer, as confirmed by the X-

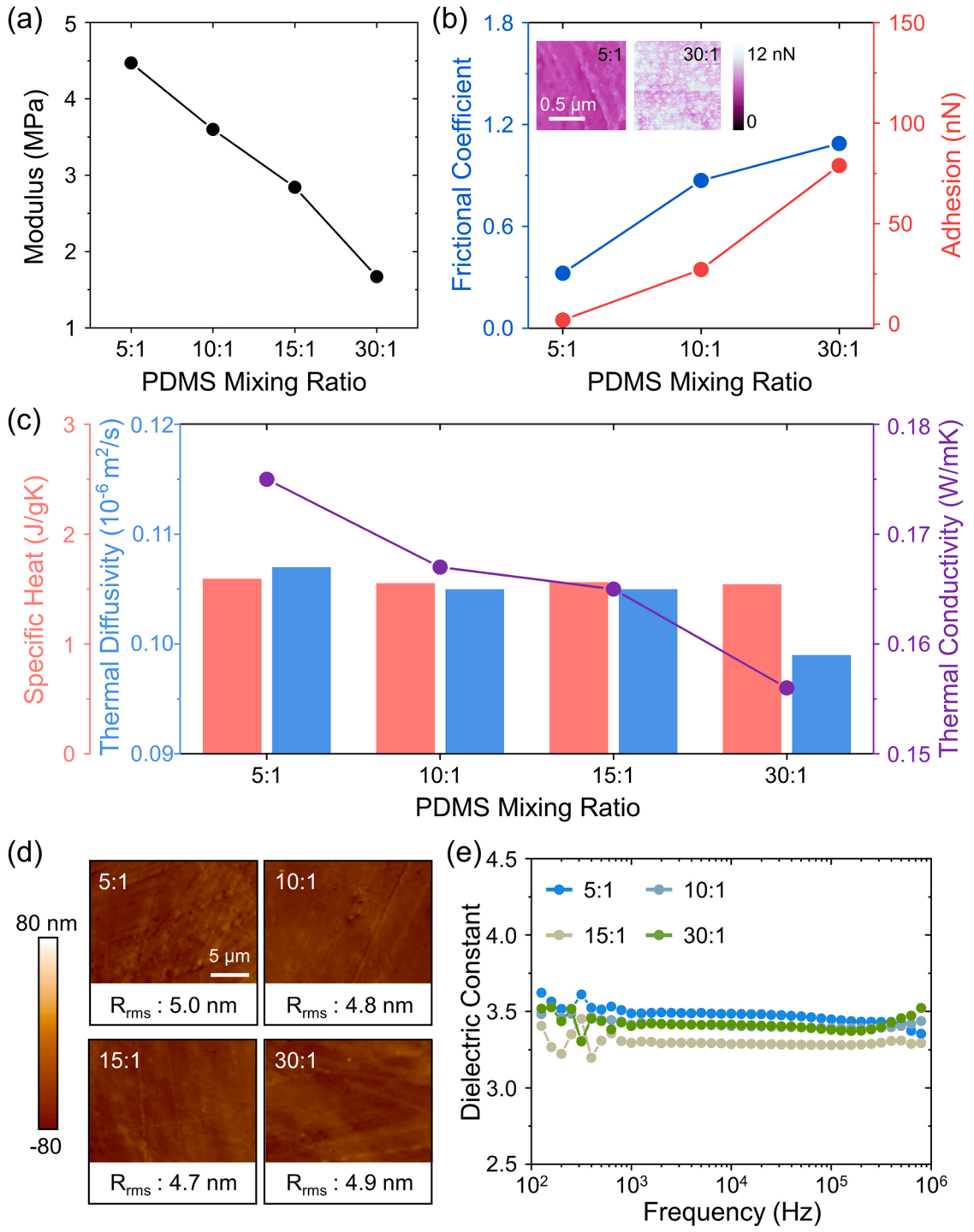

Fig. 2. Mechanical, thermal, morphological, and dielectric properties of PDMS. (a) Young's modulus, (b) frictional coefficient and adhesion force, (c) specific heat, thermal diffusivity, and thermal conductivity, (d) surface morphology, and (e) dielectric constant. Here, the mixing ratio represents the weight ratio of precursor to crosslinker. In (b), the distribution of adhesion force (scan size of 1×1 μm^2) is shown for 5:1 and 30:1 mixing ratios. In (c), the thermal conductivity is obtained by multiplying heat capacity, density, and thermal diffusivity. In (d), the root-mean-square value of roughness (R_{rms}) is shown for each ratio.

ray diffraction pattern (Fig. S4, Supporting Information) [36]. Fig. 2b shows the mixing ratio-dependent frictional coefficient and adhesion force of the PDMS polymers. In contrast to Young's modulus, both the frictional coefficient and adhesion force increase with increasing mixing ratio. Such changes are likely to be related to the increased softness and stickiness, as evidenced by the significantly increased force-distance hysteresis curve for a high mixing ratio PDMS (Fig. S5, Supporting Information). Increased softness causes increased contact area for the external force; hence, the lateral frictional coefficient increases accordingly. Increased stickiness causes increased force for detachment; hence, the adhesion force increases accordingly.

Fig. 2c shows the mixing ratio-dependent thermal properties of the PDMS polymers. While the specific heat is almost constant irrespective of the mixing ratio, the thermal diffusivity and conductivity decrease with increasing mixing ratio. The decreased thermal diffusivity and conductivity are attributed to the decreased density (Fig. S6, Supporting Information) and atomic vibrations due to higher amorphous content.

In contrast to the mechanical and thermal properties, the

morphological and dielectric properties of PDMS effectively remains constant. As shown in Fig. 2d,e, the surface morphology is quite similar with small variation of roughness, and the dielectric constant is almost constant over a wide frequency range irrespective of the mixing ratio. These findings suggest that PDMS polymers can be an appropriate platform to investigate the correlation between frictional heat and triboelectric charge by neglecting the effects of surface roughness and dielectric constant on triboelectrification [37].

3.3. Mixing ratio- and contact pressure-dependent triboelectric charge and temperature variation

Fig. 3a and Fig. S7, Supporting Information, show the mixing ratio-dependent open-circuit voltage, short-circuit current, and triboelectric charges of FTO-PDMS TENGs. The contact pressure was set to 0.28 N/cm^2. Apparently, the triboelectric charges increase and then become saturated with increasing sliding time. For each ratio, however, the initial increasing behavior and saturated charges are different. For the quantitative analysis, the sliding time-dependent triboelectric charge [$Q_{tribo}(t)$] is fitted (solid lines) using a simple exponential decay

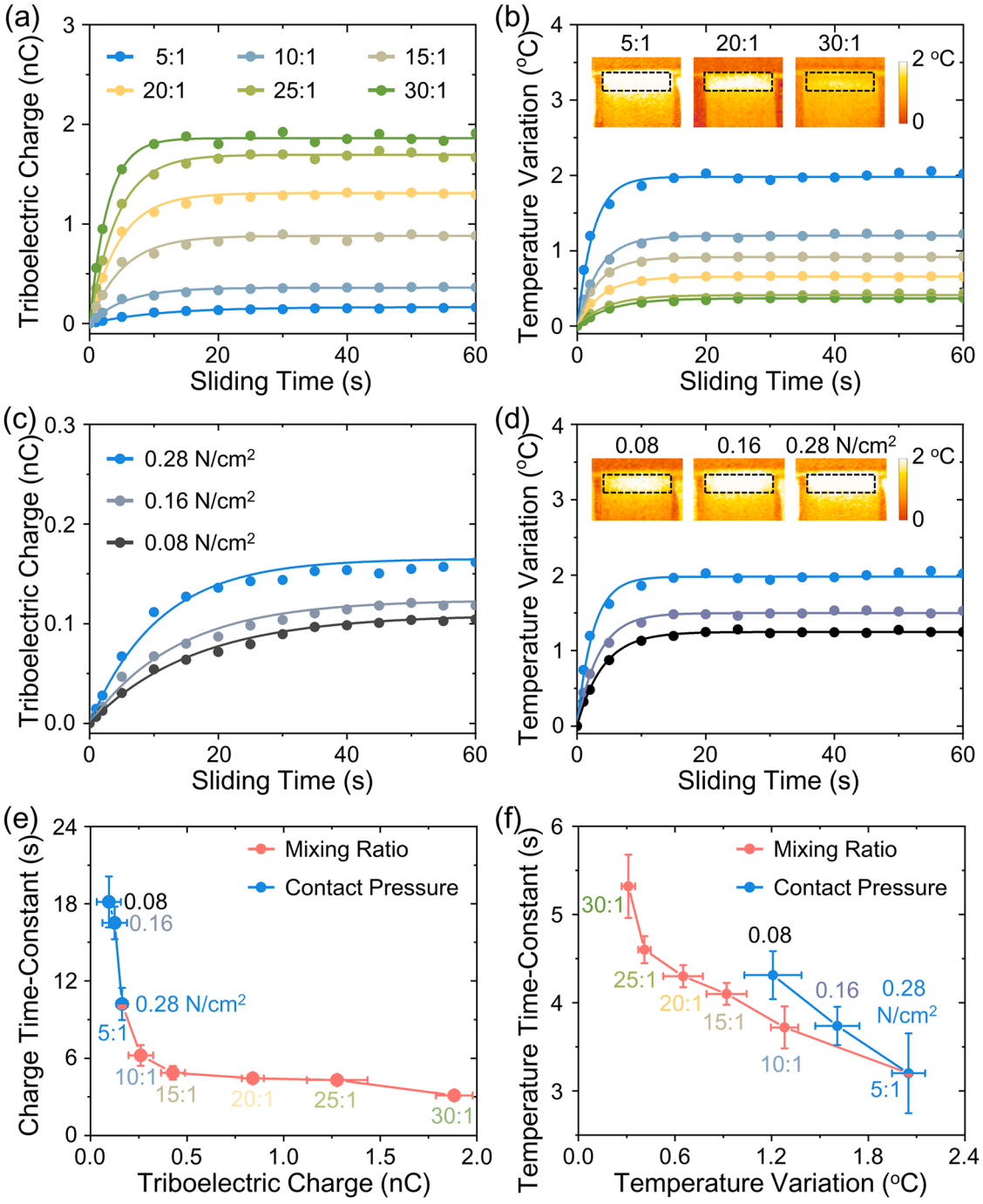

Fig. 3. Mixing ratio- and contact pressure-dependent triboelectric charge and temperature variation. Sliding time-dependent triboelectric charge and temperature variation of PDMS for various (a,b) mixing ratios and (c,d) contact pressures. Solid lines represent the fitting curves of a simple exponential decay function. In (b,d), the infrared (IR) images are selectively shown. Relationship between (e) saturated triboelectric charge and charge time-constant, and (f) saturated temperature variation and temperature time-constant for various mixing ratios (red circles) and contact pressures (blue circles).

function, i.e.,

$$Q_{tribo}(t) = Q_{tribo}(\infty)\left[1 - \exp\left(-\frac{t}{\tau_C}\right)\right] \quad (1)$$

where $Q_{tribo}(\infty)$ and τ_C represent the saturated triboelectric charge and the charge time-constant, respectively. Note that a simple exponential decay function has been predicted in a model of TENG and frequently observed for time-dependent charging/discharging in numerous triboelectric systems [38].

Fig. 3b and Fig. S8, Supporting Information, show the mixing ratio-dependent temperature variations of PDMS and FTO, respectively. IR camera images are also shown in Fig. 3b and Fig. S9, Supporting Information. Similar to the triboelectric charge, the temperatures increase and then become saturated with different initial increasing behavior and saturated temperature. Overall, the saturated temperature of FTO is lowered than that of PDMS, probably due to the underlying thick glass substrate. Intriguingly, the saturated temperature of PDMS is highest for the 5:1 mixing ratio, at which the saturated triboelectric charge is smallest. The sliding time-dependent temperature $[T_{tribo}(t)]$ is fitted (solid lines) using a simple exponential decay function, i.e.,

$$T_{tribo}(t) = T_{tribo}(\infty)\left[1 - \exp\left(-\frac{t}{\tau_T}\right)\right] \quad (2)$$

where $T_{tribo}(\infty)$ and τ_T represent the saturated temperature and the temperature time-constant, respectively. Note that a simple exponential decay function has been predicted in a lumped heat capacity model and frequently observed for time-dependent heating/cooling in numerous heat-transfer systems [39].

Fig. 3c,d and Fig. S10,S11, Supporting Information, show the contact pressure-dependent triboelectric charge and temperature variation, respectively. The mixing ratio was set to 5:1. The triboelectric charges and temperatures follow the similar trends as those for mixing ratio. Notably, both the saturated charge and temperature are highest at the highest pressure of 0.28 N/cm^2. The sliding time-dependent triboelectric charge and temperature are reasonably fitted by simple exponential decay functions, as denoted by solid lines.

Fitting parameters for triboelectric charge and temperature variation are shown in Fig. 3e,f, respectively, for various mixing ratios (red circles) and contact pressures (blue circles). The saturated triboelectric charges increase with increasing mixing ratio and contact pressure. The increased charges result in the decreased charge time-constant, accordingly. Note that the largest triboelectric charge and shortest charge time-constant occur at the 30:1 mixing ratio, which has the smallest Young's modulus, and largest frictional coefficient and adhesion force.

In contrast, the saturated temperature variation for PDMS decreases with increasing mixing ratio, but increases with increasing contact pressure. The increased temperature results in the decreased time-constant, accordingly. Note that the highest temperature and shortest temperature time-constant occur at the 5:1 mixing ratio, which has the largest thermal diffusivity and thermal conductivity. It is intriguing that

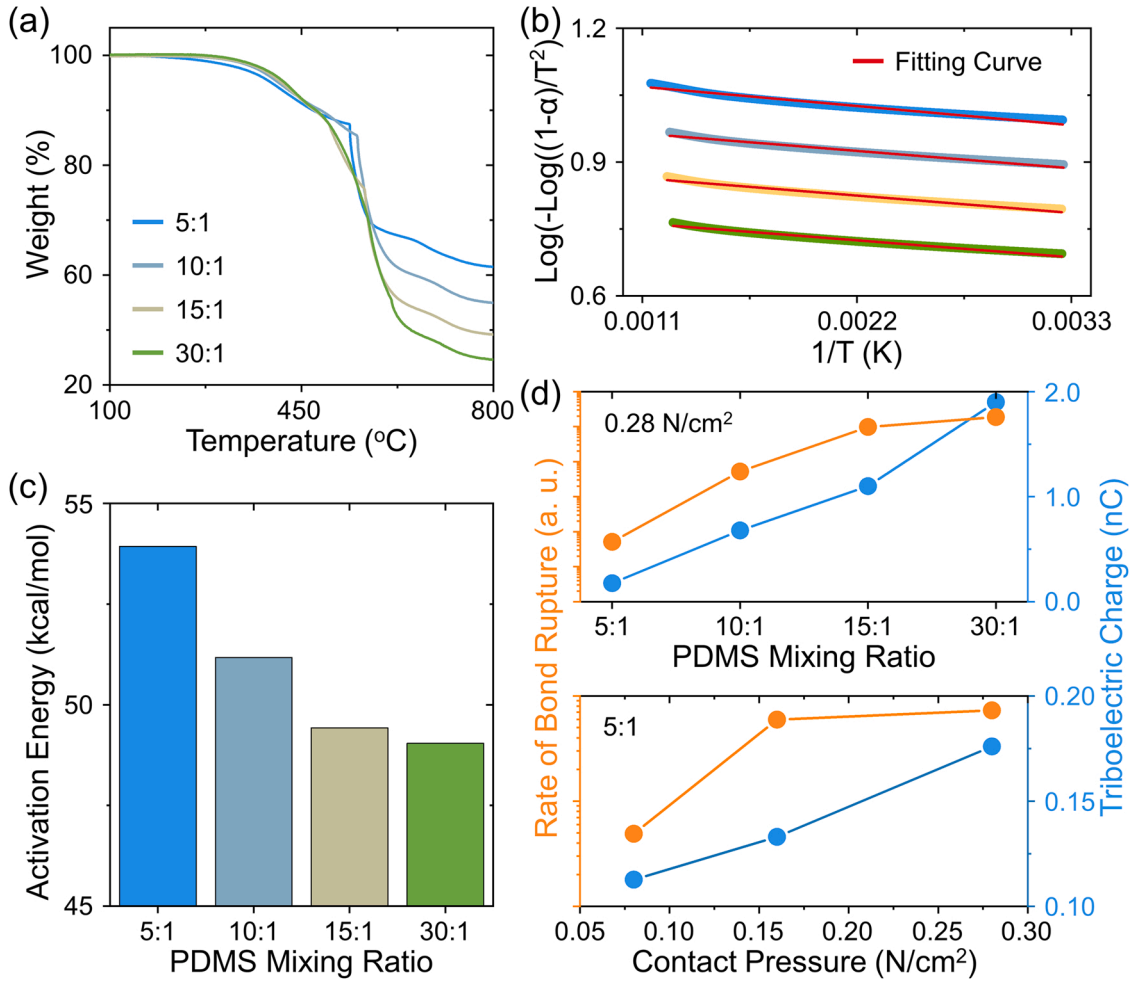

Fig. 4. Close relationship between the rate of bond rupture event and triboelectric charge. (a) Thermogravimetric analysis heating thermogram, (b) fitting curves of the Coats and Redfern equation, and (c) activation energy of PDMS polymers. (d) Mixing ratio- and contact pressure-dependent rate of bond rupture events and triboelectric charge. For mixing ratio-dependence, the contact pressure is fixed at 0.28 N/cm^2. For contact pressure-dependence, the mixing ratio is fixed at 5:1.

the triboelectric charge becomes maximized when the temperature variation of PDMS is smallest. The temperature time-constant is shorter than the charge time-constant for all contact pressures.

3.4. Effects of activation energy and contact pressure on the rate of bond rupture events

In order to understand the intriguing triboelectric charge behavior, mixing ratio-dependent thermogravimetric analysis is performed and shown the results in Fig. 4a. All of the PDMS polymers lose weight with increasing temperature. The weight losses are 60% and 45% for the 30:1 and 5:1 mixing ratios, respectively, at 800 °C. The thermogravimetric results are used to estimate the activation energy (E_a) of thermal degradation via the Coats and Redfern equation [40,41], i.e.,

$$log_{10}\left(-log_{10}\left[\frac{(1-\alpha)}{T^2}\right]\right) = A - \frac{E_a}{2.3RT} \quad (3)$$

where α, T, A, and R represent the extent of reaction, absolute temperature, proportional constant, and gas constant, respectively. The extent of reaction (α) can be written as $\alpha = \frac{m_0 - m_t}{m_0 - m_\infty}$, where m_0, m_t, and m_∞ represent the initial mass, mass at time t, and mass at the end of the reaction, respectively. The thermogravimetric data are well-fitted by Eq. (3) for all of the PDMS polymers (Fig. 4b). Fig. 4c shows that the activation energy of PDMS decreases from 54 kcal/mol at the 5:1 and 49 kcal/mol at the 30:1 mixing ratio.

According to the kinetics of mechanochemistry, the rate of bond rupture event (K) occurring in the polymer depends on the activation energy (E_A) of bond rupture and stress [42], i.e.,

$$K = K_0 \exp\left(-\frac{E_A - \beta\sigma}{RT}\right) \quad (4)$$

where K_0, β, and σ represent the Arrhenius frequency factor, proportional coefficient, and tensile stress, respectively. Based on the similar activation energies for thermal degradation and bond rupture [43,44], the mixing ratio- and contact pressure-dependent rate of bond rupture events are shown in Fig. 4d. While there is a slight deviation, the rate of bond rupture event is proportional to the triboelectric charge, which suggests a close relationship between them.

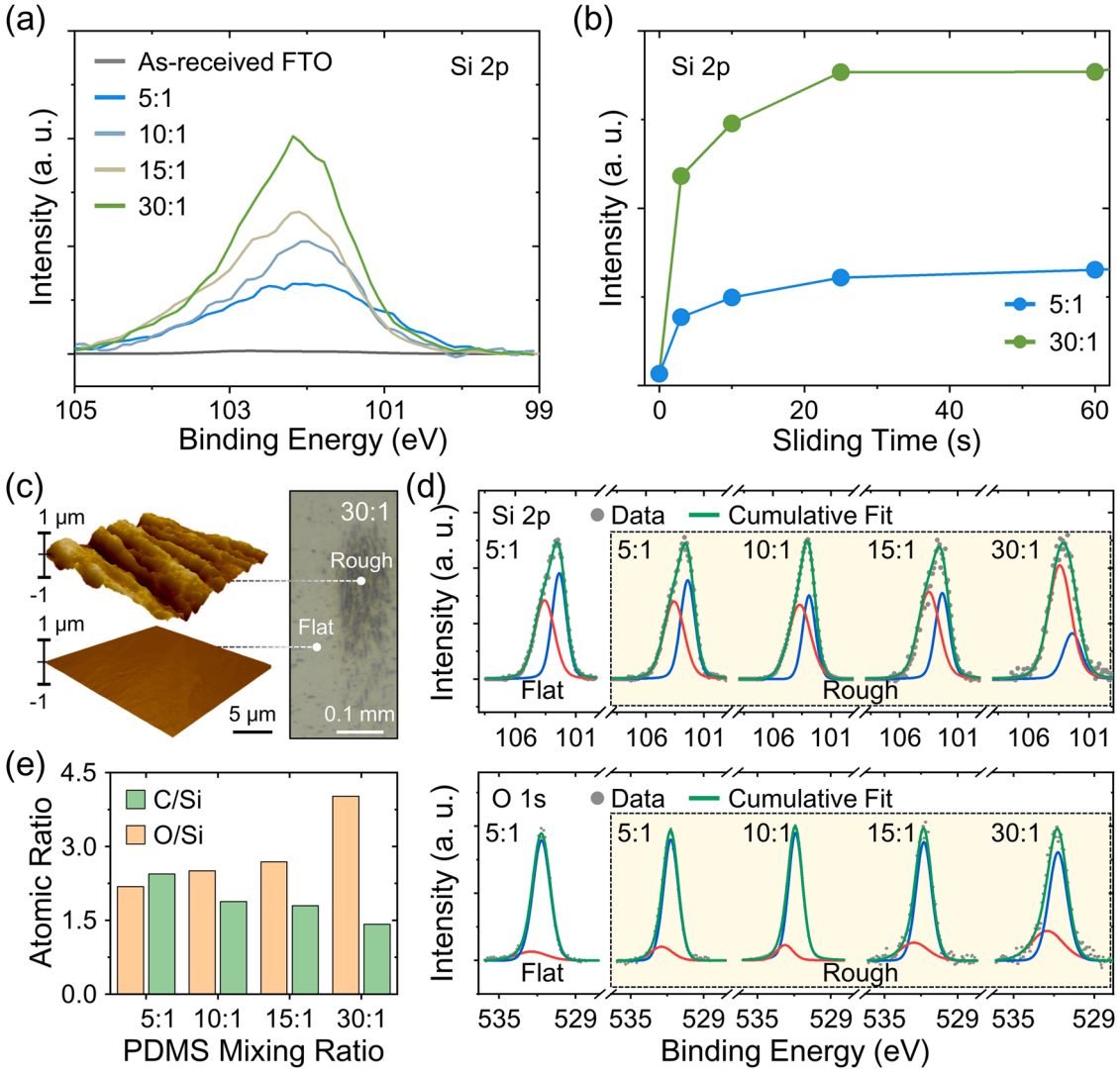

Fig. 5. X-ray photoemission investigation of bond modification and material-transfer. X-ray photoemission Si 2p intensity of FTO for various (a) mixing ratios and (b) sliding times. The sliding time is fixed at 30 s in (a), and the mixing ratio is fixed at 5:1 and 30:1 in (b). (c) Optical microscopy and atomic force microscopy images of the 30:1 after sliding. (d) Photoemission Si 2p and O 1s spectra of PDMS at flat and rough areas. For flat area, the spectra are only shown for 5:1. The blue and red curves in the Si 2p correspond to Si-O and O-Si-O peaks, respectively. The blue and red curves in the O 1s correspond to Si-O-Si and Si-OH peaks, respectively. (e) Atomic ratio of C/Si and O/Si for 5:1, 10:1, 15:1, and 30:1 mixing ratios.

3.5. X-ray photoemission investigation of bond modification/rupture and material-transfer

Surface-sensitive X-ray photoemission spectroscopy is investigated to elucidate the detailed bond rupture in PDMS. Fig. 5a,b show the Si 2p X-ray photoemission spectra of FTO with the variation of mixing ratio and sliding time, respectively. Detailed sliding time-dependent Si 2p spectra of FTO are shown in Fig. S12, Supporting Information. After sliding, the Si 2p peak drastically increases with increasing mixing ratio. In addition, the peak increases and becomes saturated with increasing sliding time for both the 5:1 and 30:1 mixing ratios. Importantly, the Si 2p peak intensities of FTO are almost linearly proportional to the corresponding triboelectric charge, as confirmed by Fig. S13, Supporting Information. Such consistency unambiguously indicates that the broken Si bonds (and charged materials) in PDMS are transferred to FTO and is participated in triboelectrification, as similarly reported for soft polymers [26,45]. As demonstrated in optical microscopy and scanning electron microscopy images (Fig. S14, Supporting Information), the PDMS residues are clearly observable in FTO after sliding.

Fig. 5c and Fig. S15, Supporting Information, show the optical microscopy and atomic force microscopy images of PDMS after sliding. Homogenous PDMS surface changes into inhomogenous for all mixing ratios, and such behavior becomes serious for the high mixing ratio. Micrometer-sized scanning X-ray photoemission spectroscopy is performed for the detailed investigation of bond modification in PDMS after sliding. The scanning is performed along the flat and rough surface, and shown the results in Fig. 5d and Fig. S16a,b, Supporting Information. As a representative, we showed the spectra at the flat area only for the 5:1 mixing ratio in Fig. 5d. Apparently, the Si 2p and O 1s spectra are different for each area, even for the same mixing ratio. In the Si 2p spectra [46], the Si-O peak decreases whereas the O-Si-O peak increases at a rough area, as compared with those at a flat area. In the O 1s spectra [47], the Si-O-Si peak decreases whereas the Si-OH peak increases at a rough area, as compared with those at a flat area. Such modifications are significant at the high mixing ratio, as clearly shown in Fig. S16c,d, Supporting Information.

The chemical compositions of PDMS are also changed, along with the spectral changes. Fig. 5e shows that the O/Si atomic ratio increases, whereas the C/Si decreases, with increasing mixing ratio. These results indicate that Si-C and Si-CH_3 bonds are inhomogeneously broken and desorbed, and Si radicals react with O and OH ions in the atmosphere, as similarly reported for plasma-treated PDMS [47,48]. This fact also implies that the bond modification, and hence triboelectric output, should depend on the atmosphere during the sliding [49].

3.6. Distributive role of frictional heat on bond rupture and temperature variation

Based on the above *in operando* and X-ray photoemission measurements, Fig. 6a shows a schematic diagram for the distributive role of frictional heat on the bond rupture and temperature variation. When the FTO slides across the PDMS surface, frictional heat is generated at the interface. The frictional heat seems to focus at certain areas due to the small thermal diffusivity/conductivity of PDMS. In addition, the activation energy of PDMS seems to be reduced due to the fast sliding induced increased heating rate [50]. A portion of frictional heat is used for bond rupture in the PDMS and the remaining portion for temperature variation in the PDMS and FTO. When the activation energy is low (such as the 30:1), a large amount of heat is used for bond breaking, and a small amount for temperature variation, and vice versa for a high activation energy (such as the 5:1). Therefore, the triboelectric charge for the 30:1 is larger than that for the 5:1, and the temperature of PDMS is lower for the former than that for the latter, as consistent with Fig. 3a,b. Note that the frictional heat itself increases with increasing contact pressure and frictional coefficient. Therefore, both the triboelectric charge and temperature variation increase with increasing contact pressure, as consistent with Fig. 3c,d. In addition, the temperature variation of FTO increases with increasing mixing ratio due to the increased frictional coefficient, as consistent with Fig. S8, Supporting Information.

The broken bonds and/or charged materials in PDMS are transferred to FTO during sliding, as schematically shown in Fig. 6b. The amount of charged material-transfer depends on the modulus (e.g., Young's) difference between FTO and PDMS [26]. Consistent with Figs. 3a,5a, the triboelectric charge of FTO-PDMS TENGs and the Si 2p peak of FTO become significant with decreasing Young's modulus of PDMS (i.e., increasing mixing ratio). This result implies that polymers with low Young's modulus, like soft styrene-ethylene/butylene-styrene copolymer, should result in higher triboelectric output in metal-polymer TENGs [26].

3.7. Advantages of in operando triboelectric charge and temperature variation measurements for understanding the triboelectrification mechanism

In operando triboelectric charge and temperature variation measurements can provide important insights into triboelectrification. First, the thermal property of contacting materials plays an important role on the triboelectric charge, as similarly proposed in a recent theory [51]. When thermal diffusivity/conductivity is small, frictional heat is

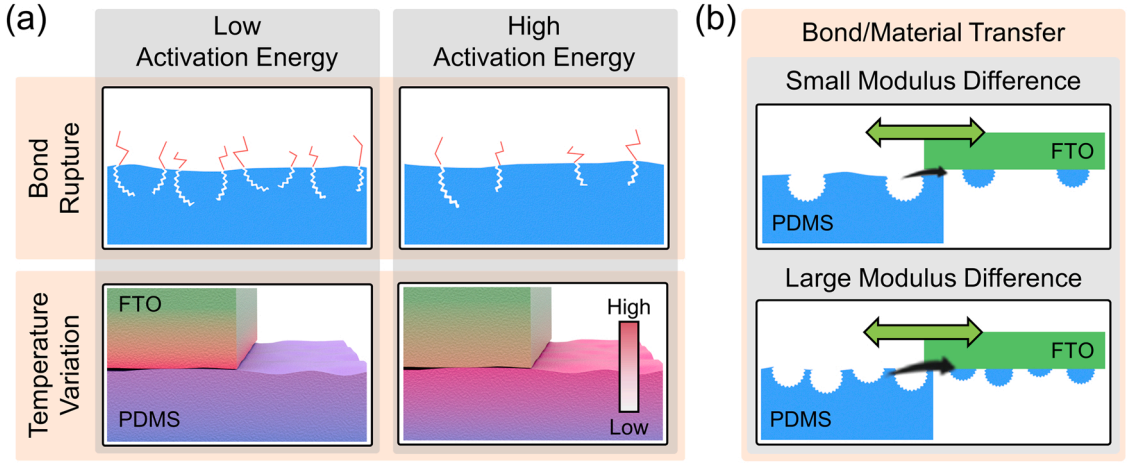

Fig. 6. Schematic illustration of distributive role of frictional heat and bond/material-transfer. (a) Bond rupture in PDMS and temperature variation of FTO and PDMS with respect to activation energy and (b) broken bond and charged material-transfer from PDMS to FTO with respect to modulus difference.

localized at certain areas of surface; which causes the significant and local bond rupture event. This claim explains the inverse proportion of triboelectric charge and temperature variation with respect to mixing ratio, local bond modification at the rough area, and the large fluctuation of local temperatures at high mixing ratio (Fig. S17, Supporting Information). In addition, this result implies that polymers with small thermal conductivity, like polyimide, should result in higher triboelectric output in metal-polymer TENGs [52]. Second, the temperature variation of two contacting materials can be used for quantifying the frictional heat. As well-documented [26], the frictional heat plays a critical role on bond rupture in polymers for the charged material-transfer induced triboelectrification. Since each chemical bond has a certain binding energy, a quantitative estimation of frictional heat can specify the bonds involved in triboelectrification. Third, the real-time and *in operando* temperature variation of two contacting materials can provide helpful information for the temperature difference induced charge-transfer model [27]. According to this model, the electrons are thermally excited and transferred from a hotter surface to a cooler one. Simultaneously obtained time-constants for triboelectric charge and temperature provide a detailed charge-transfer process after physical contact. Fourth, a similar *in operando* system can also be applicable to the physical contact of two polymers. Considering the variety of polymers with different triboelectric series, thermal conductivity, electrical conductivity, and mechanical modulus, the polymer-polymer contact would provide a significant forward step for the fundamental understanding of triboelectrification phenomena and the technological guideline for high power generation of TENGs.

4. Conclusions

In summary, *in operando* temperature variation measurement is reported to elucidate the correlation between frictional heat and triboelectric charge during the physical contact of FTO metal and PDMS polymer. Thermocouple and synchronized IR camera are used for simultaneous temperature measurement, and the mixing ratio and contact pressure are varied for systematic triboelectric charge measurement. In contrast to surface morphology and dielectric constant, the mechanical and thermal properties of PDMS are varied with mixing ratio. Namely, the Young's modulus of PDMS significantly decreases with increasing mixing ratio, whereas the frictional coefficient and adhesion force increase. The thermal diffusivity and thermal conductivity of PDMS decrease with increasing the mixing ratio, whereas the specific heat is quite similar. Detailed *in operando* investigation reveals that both triboelectric charge and temperature increase and become saturated with increasing sliding time. Intriguingly, the saturated triboelectric charge increases with increasing mixing ratio, whereas the saturated temperature decreases. On the other hand, both the saturated charge and temperature increase with increasing contact pressure. The time-constants for charge and temperature are inversely proportional to the saturated triboelectric charge and temperature, respectively. Intriguingly, the time-constant for temperature is smaller than that for triboelectric charge. Surface-sensitive X-ray photoemission spectroscopy reveals that the inhomogeneous bond modification and charged material-transfer increase with increasing mixing ratio and sliding time. These results imply that frictional heat plays a distributive role on bond rupture and temperature variation, i.e., the increased heat for the former causes the decreased heat for the latter, and vice versa. The frictional heat becomes increased due to the contact pressure and frictional coefficient, which results in the increased bond rupture and temperature variation. *In operando* temperature variation measurement can provide insight into triboelectrification by suggesting a localized heat enhanced bond rupture event, by identifying chemical bonds in a bond breaking/creation model, and by providing a detailed electron-transfer process in a thermionic emission model.

CRediT authorship contribution statement

Dong Woo Lee: Conceptualization, Validation, Investigation, Writing – original draft. **Dae Sol Kong:** Conceptualization, Validation, Investigation, Writing – original draft. **Jong Hun Kim:** Conceptualization, Validation, Investigation, Writing – original draft. Writing - review & editing. **Sang Hyeok Park:** Validation, Investigation. **Ying Chieh Hu:** Validation, Investigation. **Young Joon Ko:** Validation, Investigation. **Chan Bae Jeong:** Validation, Investigation. **Seoku Lee:** Validation, Investigation. **Joong Il Jake Choi:** Validation, Data curation, Resources. **Gwan-Hyoung Lee:** Validation, Data curation, Resources. **Minbaek Lee:** Validation, Data curation, Resources. **Jeong Jae Wie:** Validation, Data curation, Resources. **Ki Soo Chang:** Validation, Data curation, Resources. **Jeong Young Park:** Validation, Data curation, Resources. **Jong Hoon Jung:** Conceptualization, Supervision, Writing - review & editing.

Declaration of Competing Interest

The authors declare that they have no known competing financial interests or personal relationships that could have appeared to influence the work reported in this paper.

Data availability

Data will be made available on request.

Acknowledgments

This research was supported by Basic Science Research Program through the National Research Foundation of Korea (NRF), funded by the Ministry of Education, Science and Technology (2020R1A2C1006987 and 2020R1A4A1017915). J.H.K and G-H.L acknowledge the support from Basic Science Research Program through the NRF funded by the Ministry of Science, ICT & Future Planning (2018M3D1A1058793). J.Y.P acknowledge the support from the National Research Foundation of Korea (NRF) grant funded by the Korean government (MSIT) (2022R1A2C3004242).

Appendix A. Supporting information

Supplementary data associated with this article can be found in the online version at doi:10.1016/j.nanoen.2022.107813.

References

[1] G. Boyle, Renewable Energy: Power for a Sustainable Future, Oxford University Press, Oxford, 2012.
[2] D.S. Ginley, D. Cahen, Fundamentals of Materials for Energy and Environmental Sustainability, Cambridge University Press, New York, 2011.
[3] F.R. Fan, Z.Q. Tian, Z.L. Wang, Flexible triboelectric generator, Nano Energy 1 (2012) 328–334, https://doi.org/10.1016/j.nanoen.2012.01.004.
[4] Z.L. Wang, Triboelectric nanogenerators as new energy technology for self-powered systems and as active mechanical and chemical sensors, ACS Nano 7 (2013) 9533–9557, https://doi.org/10.1021/nn404614z.
[5] A. Ahmed, I. Hassan, M.F. El-Kady, A. Radhi, C.K. Jeong, P.R. Selvaganapathy, J. Zu, S. Ren, Q. Wang, R.B. Kaner, Integrated triboelectric nanogenerators in the era of the Internet of Things, Adv. Sci. 6 (2019), 1802230, https://doi.org/10.1002/advs.201802230.
[6] H. Wu, W. He, C. Shan, Z. Wang, S. Fu, Q. Tang, H. Guo, Y. Du, W. Liu, C. Hu, Achieving remarkable charge density via self-polarization of polar high-k material in a charge-excitation triboelectric nanogenerator, Adv. Mater. 34 (2022), 2109918, https://doi.org/10.1002/adma.202109918.
[7] H.S. Kim, S. Hur, D.-G. Lee, J.-C. Shin, H. Qiao, S. Mun, H. Lee, W. Moon, Y. Kim, J. M. Baik, C.-Y. Kang, J.H. Jung, H.-C. Song, Ferroelectrically augmented contact electrification enables efficient acoustic energy transfer through liquid and solid media, Energy Environ. Sci. 15 (2022) 1243–1255, https://doi.org/10.1039/D1EE02623B.
[8] A. Šutka, K. Mālnieks, A. Linarts, M. Timusk, V. Jurķāns, I. Gorņevs, J. Blūms, A. Bērziņa, U. Joost, M. Knite, Inversely polarised ferroelectric polymer contact electrodes for triboelectric-like generators from identical materials, Energy Environ. Sci. 11 (2018) 1437–1443, https://doi.org/10.1039/C8EE00550H.

[9] X. Chen, Y. Zhao, F. Wang, D. Tong, L. Gao, D. Li, L. Wu, X. Mu, Y. Yang, Boosting output performance of triboelectric nanogenerator via mutual coupling effects enabled photon-carriers and plasmon, Adv. Sci. 9 (2022), 2103957, https://doi.org/10.1002/advs.202103957.
[10] J. Fu, G. Xu, C. Li, X. Xia, D. Guan, J. Li, Z. Huang, Y. Zi, Achieving ultrahigh output energy density of triboelectric nanogenerators in high-pressure gas environment, Adv. Sci. 7 (2020), 2001757, https://doi.org/10.1002/advs.202001757.
[11] R. Wen, J. Guo, A. Yu, J. Zhai, Z.L. Wang, Humidity-resistive triboelectric nanogenerator fabricated using metal organic framework composite, Adv. Funct. Mater. 29 (2019), 1807655, https://doi.org/10.1002/adfm.201807655.
[12] M. He, W. Du, Y. Feng, S. Li, W. Wang, X. Zhang, A. Yu, L. Wan, J. Zhai, Flexible and stretchable triboelectric nanogenerator fabric for biomechanical energy harvesting and self-powered dual-mode human motion monitoring, Nano Energy 86 (2021), 106058, https://doi.org/10.1016/j.nanoen.2021.106058.
[13] X. Xia, H. Wang, H. Guo, C. Xu, Y. Zi, On the material-dependent charge transfer mechanism of the contact electrification, Nano Energy 78 (2020), 105343, https://doi.org/10.1016/j.nanoen.2020.105343.
[14] F. Shen, D. Zhang, Q. Zhang, Z. Li, H. Guo, Y. Gong, Y. Peng, Influence of temperature difference on performance of solid-liquid triboelectric nanogenerators, Nano Energy 99 (2022), 107431, https://doi.org/10.1016/j.nanoen.2022.107431.
[15] X. Zhao, X. Lu, Q. Zheng, L. Fang, L. Zheng, X. Chen, Z.L. Wang, Studying of contact electrification and electron transfer at liquid-liquid interface, Nano Energy 87 (2021), 106191, https://doi.org/10.1016/j.nanoen.2021.106191.
[16] D.J. Lacks, T. Shinbrot, Long-standing and unresolved issues in triboelectric charging, Nat. Rev. Chem. 3 (2019) 465–476, https://doi.org/10.1038/s41570-019-0115-1.
[17] C. Liu, A.J. Bard, Electrons on dielectrics and contact electrification, Chem. Phys. Lett. 480 (2009) 145–156, https://doi.org/10.1016/j.cplett.2009.08.045.
[18] S. Pan, Z. Zhang, Triboelectric effect: a new perspective on electron transfer process, J. Appl. Phys. 122 (2017), 144302, https://doi.org/10.1063/1.5006634.
[19] L.S. Mccarty, G.M. Whitesides, Electrostatic charging due to separation of ions at interfaces: contact electrification of ionic electrets, Angew. Chem. Int. Ed. 47 (2008) 2188–2207, https://doi.org/10.1002/anie.200701812.
[20] A.F. Diaz, D. Wollmann, D. Dreblow, Contact electrification: ion transfer to metals and polymers, Chem. Mater. 3 (1991) 997–999, https://doi.org/10.1021/cm00018a006.
[21] J. Lowell, The role of material transfer in contact electrification, J. Phys. D. Appl. Phys. 10 (1977) L233–L235, https://doi.org/10.1088/0022-3727/10/17/001.
[22] H.T. Baytekin, A.Z. Patashinski, M. Branicki, B. Baytekin, S. Soh, B.A. Grzybowski, The mosaic of surface charge in contact electrification, Science 333 (2011) 308–312, https://doi.org/10.1126/science.1201512.
[23] D. Li, C. Xu, Y. Liao, W. Cai, Y. Zhu, Z.L. Wang, Interface inter-atomic electron-transition induced photon emission in contact-electrification, Sci. Adv. 7 (2021) eabj0349, https://doi.org/10.1126/sciadv.abj0349.
[24] S. Lin, L. Xu, L. Zhu, X. Chen, Z.L. Wang, Electron transfer in nanoscale contact electrification: photon excitation effect, Adv. Mater. 31 (2019), 1901418, https://doi.org/10.1002/adma.201901418.
[25] H.T. Baytekin, B. Baytekin, J.T. Incorvati, B.A. Grzybowski, Material transfer and polarity reversal in contact charging, Angew. Chem. Int. Ed. 51 (2012) 4843–4847, https://doi.org/10.1002/anie.201200057.
[26] A. Šutka, K. Mālnieks, L. Lapčinskis, P. Kaufelde, A. Linarts, A. Bērziņa, R. Zābels, V. Jurķāns, I. Gorņevs, J. Blūms, M. Knite, The role of intermolecular forces in contact electrification on polymer surfaces and triboelectric nanogenerators, Energy Environ. Sci. 12 (2019) 2417–2421, https://doi.org/10.1039/c9ee01078e.
[27] C. Xu, Y. Zi, A.C. Wang, H. Zou, Y. Dai, X. He, P. Wang, Y.-C. Wang, P. Feng, D. Li, Z.L. Wang, On the electron-transfer mechanism in the contact-electrification effect, Adv. Mater. 30 (2018), 1706790, https://doi.org/10.1002/adma.201706790.
[28] B. Jayasena, S.N. Melkote, An investigation of PDMS stamp assisted mechanical exfoliation of large area graphene, Procedia Manuf. 1 (2015) 840–853, https://doi.org/10.1016/j.promfg.2015.09.073.
[29] H. Kim, S. Choi, Y. Hong, J. Chung, J. Choi, W.-K. Choi, I.W. Park, S.H. Park, H. Park, W.-J. Chung, K. Heo, M. Lee, Biocompatible and biodegradable triboelectric nanogenerators based on hyaluronic acid hydrogel film, Appl. Mater. Today 22 (2021), 100920, https://doi.org/10.1016/j.apmt.2020.100920.
[30] J.H. Kim, D. Fu, S. Kwon, K. Liu, J. Wu, J.Y. Park, Crossing thermal lubricity and electronic effects in friction: vanadium dioxide under the metal–insulator transition, Adv. Mater. Interfaces 3 (2016), 1500388, https://doi.org/10.1002/admi.201500388.
[31] J.H. Kim, S. Youn, T.W. Go, J. Kim, C. Yoo, M.S. Shawkat, S.S. Han, S.-J. Jeon, Y. Jung, J.Y. Park, W. Lee, Revealing Pt-seed-induced structural effects to tribological/electrical/thermoelectric modulations in two-dimensional $PtSe_2$ using scanning probe microscopy, Nano Energy 91 (2022), 106693, https://doi.org/10.1016/j.nanoen.2021.106693.
[32] K. Deng, W.H. Ko, J. A study of static friction between silicon and silicon compounds, Micromech. Microeng. 2 (1992) 14–20, https://doi.org/10.1088/0960-1317/2/1/004/meta.
[33] K. Shinzato, T. Baba, A laser flash apparatus for thermal diffusivity and specific heat capacity measurements, J. Therm. Anal. Calor. 64 (2001) 413–422, https://doi.org/10.1023/A:1011594609521.
[34] A.F. Diaz, R.M. Felix-Navarro, A semi-quantitative tribo-electric series for polymeric materials: the influence of chemical structure and properties, J. Electrost. 62 (2004) 277–290, https://doi.org/10.1016/j.elstat.2004.05.005.
[35] A.C.C. Esteves, J. Brokken-Zijp, J. Laven, H.P. Huinink, N.J.W. Reuvers, M.P. Van, G. de With, Influence of cross-linker concentration on the cross-linking of PDMS and the network structures formed, Polymer 31 (2009) 3955–3966, https://doi.org/10.1016/j.polymer.2009.06.022.
[36] L.H. Sperling, Introduction to Physical Polymer Science, John Wiley & Sons, New York, 1992.
[37] S. Liu, S. Wang, L. Lin, Y. Liu, Y.S. Zhou, Y. Hu, Z.L. Wang, Theoretical study of contact-mode triboelectric nanogenerators as an effective power source, Energy Environ. Sci. 6 (2013) 3576–3583, https://doi.org/10.1039/C3EE42571A.
[38] S. Niu, Z.L. Wang, Theoretical systems of triboelectric nanogenerators, Nano Energy 14 (2015) 161–192, https://doi.org/10.1016/j.nanoen.2014.11.034.
[39] F.P. Incropera, D.P. DeWitt, Fundamentals of Heat and Mass Transfer, John Wiley & Sons, New York, 2002.
[40] A.W. Coats, J.P. Redfern, Kinetic parameters from thermogravimetric data, Nature 201 (1964) 68–69, https://doi.org/10.1038/201068a0.
[41] T.S. Radhakrishnan, New method for evaluation of kinetic parameters and mechanism of degradation from pyrolysis–GC studies: Thermal degradation of polydimethylsiloxanes, J. Appl. Polym. Sci. 73 (1999) 441–450, https://doi.org/10.1002/(SICI)1097-4628(19990718)73:3<441::AID-APP16>3.0.CO;2-J.
[42] M.K. Beyer, H. Clausen-Schaumann, Mechanochemistry: the mechanical activation of covalent bonds, Chem. Rev. 105 (2005) 2921–2948, https://doi.org/10.1021/cr030697h.
[43] S.N. Zhurkov, Kinetic concept of the strength of solids, Int. J. Fract. 26 (1984) 295–307, https://doi.org/10.1007/bf00962961.
[44] S.N. Zhurkov, V.E. Korsukov, Atomic mechanism of fracture of solid polymers, J. Polym. Sci. B 12 (1974) 385–398, https://doi.org/10.1002/pol.1974.180120211.
[45] R.K. Pandey, H. Kakehashi, H. Nakanishi, S. Soh, Correlating material transfer and charge transfer in contact electrification, J. Phys. Chem. C. 122 (2018) 16154–16160, https://doi.org/10.1021/acs.jpcc.8b04357.
[46] B.K. Yun, J.W. Kim, H.S. Kim, K.W. Jung, Y. Yi, M.-S. Jeong, J.-H. Ko, J.H. Jung, Base-treated polydimethylsiloxane surfaces as enhanced triboelectric nanogenerators, Nano Energy 15 (2015) 523–529, https://doi.org/10.1016/j.nanoen.2015.05.018.
[47] Y. Ohkubo, K. Endo, K. Yamamura, Adhesive-free adhesion between heat-assisted plasma-treated fluoropolymers (PTFE, PFA) and plasma-jet-treated polydimethylsiloxane (PDMS) and its application, Sci. Rep. 8 (2018) 18058, https://doi.org/10.1038/s41598-018-36469-y.
[48] C. Satriano, G. Marietta, B. Kasemo, Oxygen plasma-induced conversion of polysiloxane into hydrophilic and smooth SiO_x surfaces, Surf. Interface Anal. 40 (2008) 649–656, https://doi.org/10.1002/sia.2764.
[49] L.L. Sun, S.Q. Lin, W. Tang, X. Chen, Z.L. Wang, Effect of redox atmosphere on contact electrification of polymers, ACS Nano 14 (2020) 17354–17364, https://doi.org/10.1021/acsnano.0c07480.
[50] G. Camino, S.M. Lomakin, M. Lazzari, Polydimethylsiloxane thermal degradation Part 1. Kinetic aspects, Polymer 42 (2001) 2395–2402, https://doi.org/10.1016/S0032-3861(00)00652-2.
[51] E.-C. Shin, J.-H. Ko, H.-K. Lyeo, Y.-H. Kim, Derivation of a governing rule in triboelectric charging and series from thermoelectricity, Phys. Rev. Res. 4 (2022), 023131, https://doi.org/10.1103/PhysRevResearch.4.023131.
[52] H. Chen, V.V. Ginzburg, J. Yang, Y. Yang, W. Liu, Y. Huang, L. Du, B. Chen, Thermal conductivity of polymer-based composites: Fundamentals and applications, Prog. Polym. Sci. 59 (2016) 41–85, https://doi.org/10.1016/j.progpolymsci.2016.03.001.

Dong Woo Lee is a master's course student at department of Physics, Inha University under the supervision of Prof. Jong-Hoon Jung. He received bachelor's degree (2019) from Inha University. His current research interests are piezoelectric and triboelectric nanogenerators and their application to human body mechanical energy.

Dae Sol Kong is a PhD student at Department of Physics, Inha University under the supervision of Prof. JongHoon Jung. He received his BS degree (2018) from Inha University. His current research interests are flexoelectric effect on triboelectrification and its application to high power DC generation.

Jong Hun Kim is a research professor in Department of Materials Science and Engineering at Seoul National University. He earned his Ph.D. in Physics with scanning probe microscopy related study on local electrical properties of thin dielectric materials at Seoul National University. After graduation in 2009, he worked as a research engineer in Samsung electronics System LSI. After he moved to Korea Advanced Institute of Science and Technology as a postdoctoral fellow in 2012, he studied local tribological/electrical properties of either thin films or low-dimensional materials. After joining to Prof. Gwan-Hyoung Lee's group in 2016, he has been carrying out surface studies to reveal local electrical, mechanical properties of two-dimensional materials.

Sang Hyeok Park completed his bachelor's degree in Physics at Inha University, South Korea in 2020, He continued his M.S. program at Inha University's Department of Physics under the supervision of Prof. Minbaek Lee. His research topic is solid state physics especially in the analysis of charge trapping technique in polymeric materials. He is also investigating the applications of triboelectric and piezoelectric systems.

Young Joon Ko is a PhD student at Department of Physics, Inha University under the supervision of Prof. JongHoon Jung. He received his MS (2017) and BS degree (2015) from Inha University. His current research interests are the fundamental mechanism of triboelectrification and its application to portable electronic devices.

Chan Bae Jeong received the M.S. degree in optoelectronics and physics from Ulsan University, Ulsan, South Korea, in 2015. He is currently a Researcher with the Korea Basic Science Institute, Daejeon, South Korea. His current research interests include infrared microthermography, photothermal deflection spectroscopy, and local heat distribution analysis.

Gwan-Hyoung Lee is associate professor in Department of Materials Science and Engineering at Seoul National University. He received Ph.D. in Materials Science and Engineering from Seoul National University in 2006. During graduate school, he worked at University of Illinois at Urbana-Champaign as a visiting scholar in 2002. After graduation, he joined Samsung electronics as a senior engineer, developing LCD backlight unit and OLED devices. He moved to Columbia University as a postdoctoral research scientist in 2010. His research activities include the investigation of fundamental properties and synthesis of two-dimensional (2D) materials and van der Waals heterostructure devices for electrical and optical applications.

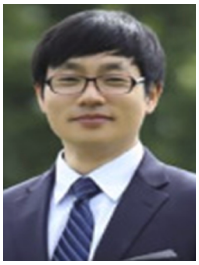

Minbaek Lee is Associated Professor in the Department of Physics at Inha University. He received his Ph.D. in Physics (2009) from Seoul National University and conducted research at Georgia Institute of Technology on energy harvesting devices based on metal oxide nanowires (ZnO NW, perovskite nanostructures) from 2009 to 2012. From 2012–2013, he worked at Samsung Electronics for the development of a new Application Processor (AP). His current research topics include triboelectricity and piezoelectricity, self-powered nano-systems, and 2D-material based device physics and their applications.

Jeong Jae Wie is currently Associate Professor in the Department of Organic and Nano Engineering and Human-Tech Convergence Program at Hanyang University, South Korea. From 2015–2022, he was on faculty at Inha University in 2015 following postdoctoral research at the United States Air Force Research Laboratory (AFRL) and at the Massachusetts Institute of Technology (MIT). He completed his Ph.D. degree in Department of Chemical Engineering from the University of Delaware in 2013. The breadth of his research interests includes soft robotics, shape reconfigurable devices, sulfur-rich polymers, and sustainable polymer composites.

Jeong Young Park currently is a professor at Department of Chemistry, Korea Advanced Institute of Science and Technology, and an associate director of Center for Nanomaterials and Chemical Reactions, Institute for Basic Science, Republic of Korea. He received his Ph.D. from Seoul National University in 1999, followed by the work as a staff scientist at Lawrence Berkeley National Laboratory. His research focuses on surface phenomena covering energy dissipation and conversion at surfaces, nanotribology, catalysis, and renewable energy conversion. He has published 310 peer-reviewed articles and book chapters in the fields of surface science and catalysis.

Ki Soo Chang received the B.S. degree in the Department of Electronic Materials and Device Engineering from Inha University in 1999 and the M.S. and Ph.D. degrees in the Department of Information and Communications from Gwangju Institute of Science & Technology (GIST) in 2002 and 2007, respectively. In 2007, he joined the Korea Basic Science Institute (KBSI), where he is presently a principal researcher. His current research interests include the development of thermal imaging microscope for semiconductor device applications and nanobiophotonic imaging systems for biomedical applications.

Jong Hoon Jung is a Professor in Department of Physics at Inha University. He received his Ph.D. from Seoul National University in Department of Physics in 2000. After working as a postdoctoral researcher at Seoul National University and Spin superstructure ERATO project in Japan Science and Technology, he joined the Department of Physics, Inha University in 2004. His recent research interest is focused on piezoelectric/pyroelectric/triboelectric nanogenerators in ferroelectric nano materials, and functional devices in flexible transition metal oxide films.